# Synthesis and Temperature-Dependence of Hydrogen-Terminated Silicon Clusters

**Gregory A. Rechtsteiner, Oliver Hampe, and Martin F. Jarrold***

*Department of Chemistry, Northwestern University, 2145 Sheridan Road, Evanston, Illinois 60208*

*Received: November 15, 2000; In Final Form: March 1, 2001*

A novel laser photolysis source has been used to synthesize hydrogen-terminated silicon clusters $Si_nH_x^+$, where $n \leq 50$. Using mass spectrometry, the hydrogen content of the $Si_nH_x^+$ clusters with $n = 10-30$ was measured as a function of temperature from 300 to 950 K. For $n = 10-22$ at the lower temperatures, there is a broad distribution of [H]/[Si] ratios which peak around compositions expected for clusters with bulklike silicon cores ($x/n > 1$). $Si_nH_x^+$ clusters with $x/n \cong 1$ appear to be favored at intermediate temperatures. This stoichiometric composition suggests three-dimensional, $Si_nH_n^+$ cage-like structures built from Si−H units. The stability of the cage geometries is supported by density functional calculations. For cluster cations with $n \geq 23$ an abrupt transition occurs and there is a sharp drop in the hydrogen content at the lower temperatures. For these clusters, $Si_nH_{(n-y)}^+$ ($y = 1-5$) compositions are prominent at the higher temperatures. These compositions suggest cage-like geometries with one or more internal silicon atoms. By adjusting the source conditions it is possible to generate $Si_nH_x^+$ ($n \geq 23$) clusters with a narrow distribution of $x$ (less than two hydrogens wide).

## Introduction

Since the discovery of visible light emission from porous silicon (PS),[1] extensive experimental and theoretical studies have been performed on materials containing nanometer-sized silicon species.[2] There have been numerous experimental and theoretical studies of small to medium-sized, hydrogen-terminated silicon clusters ($Si_nH_x$, where $1 \leq n \leq \sim 40$ and $1 \leq x \leq 2n + 2$). These investigations have probed the role $Si_nH_x$ clusters play in (i) chemical vapor deposition (CVD) and plasma enhanced chemical vapor deposition (PECVD) processes,[3−19] (ii) potential optoelectronic devices (i.e., the integration of optically active, silicon-based materials and current VLSI/ULSI technology),[20−26] and (iii) the interaction of hydrogen with bulk silicon surfaces.[27−30]

Mass spectrometry has been used to probe the hydrogen-to-silicon ratios of hydrogen-terminated silicon clusters generated using a variety of methods. A wide range of [H]/[Si] ratios have been observed, ranging from close to two to almost zero, depending on the conditions used to prepare the clusters. Using an rf glow discharge in silane ($SiH_4$) Haller observed the growth of $Si_nH_x^+$ ($n = 1-7$) clusters with a mean hydrogen-to-silicon ratio of 1.5 for $n \geq 3$.[3] Similarly, Martin and Schaber used rf discharge and thermal decomposition sources to synthesize small ($n \leq 18$) and medium ($25 \leq n \leq \sim 60$) sized $Si_nH_x^+$ cations, respectively.[4] On the basis of the mass spectra, Martin and Schaber proposed geometries based on five- and six-membered silicon rings. These building blocks allowed for the construction of several three-dimensional structures, including tetravalent silicon atoms arranged in cage-like geometries.

Murakami and Kanayama have grown $Si_nH_x^+$ ($n = 2-10$) cations in a quadrupole ion trap, and found $Si_6H_x^+$ and $Si_{10}H_x^+$ to be abundant.[24,31] Using a silane radio frequency glow discharge source, Hollenstein and co-workers reported the production of $Si_nH_x^-$ ions ($n = 1-44$).[14] Mass spectra revealed that clusters with $n > 10$ have a broad distribution of [H]/[Si] ratios with a maximum at ∼4/3. This was interpreted as being inconsistent with pure $Si_n$ cores covered with surface H atoms. In addition, Kessels and co-workers have reported the formation of small $Si_nH^+$ ($n = 1-10$) cations in an expanding argon−hydrogen−silane plasma. They suggested that the high temperature of the plasma probably results in the production of hydrogen-poor clusters.[15]

A number of theoretical studies of small- to medium-sized, hydrogen-terminated silicon clusters have also been performed in recent years. Like the experimental studies, these investigations have probed the role $Si_nH_x$ clusters play in (i) chemical vapor deposition (CVD) and plasma-enhanced chemical vapor deposition (PECVD) processes,[17,32−50] (ii) potential optoelectronic devices,[23,51−58] and (iii) modeling the interaction of hydrogen with bulk silicon surfaces.[59−64]

A wide variety of quantum-chemical methods have been used to calculate the structures, evaluate the stabilities, and explore the chemical and physical properties of hydrogen-terminated silicon clusters. Ragahavachari[33,34,36] used ab initio methods (Hartree−Fock and Moller−Plesset) to examine the clustering reactions that occur between $Si_nH_x^+$ species and silane $SiH_4$ to produce larger $Si_nH_x^+$ species. Using the same quantum-chemical methods, Michels and Hobbs[38] investigated the electronic structure and thermochemistry of silicon hydride $Si_nH^-$ anions. These studies were focused on understanding the processes that occur in CVD methods.

Recently, there have been more studies aimed at probing the structures and stability of hydrogen-terminated silicon clusters.[41,45,54,57,65] Using a global search strategy (Monte Carlo with MINDO/3), Meleshko and co-workers[57] examined the structure of small $Si_nH_x$ clusters ($n = 1-6$) containing a range of hydrogen atoms. According to these calculations, hydrogenated diamond-lattice fragments are not always the most stable $Si_nH_x$ structures; however, clusters with enough hydrogen to saturate the dangling bonds of a diamond-like fragment exhibit a diamond structure at any size. Using ab initio methods, Katzer and co-workers calculated the thermodynamic properties of $Si_nH_x$ ($n = 1-5$) clusters. Similarly, Swihart and Girshick[45]

* Author to whom correspondence should be addressed.

10.1021/jp004223n CCC: $20.00 
Published on Web 04/14/2001

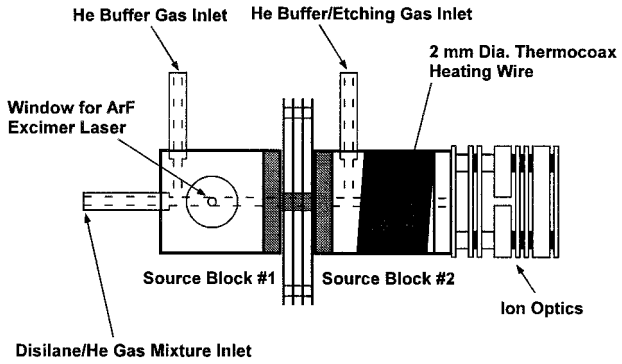


**Figure 1.** A schematic diagram of the photolysis source used for the production of $Si_nH_x$ clusters.

examined the thermochemistry and the kinetics for formation of silicon hydride clusters with 1−20 silicon atoms.

The electronic structure and optical properties of $Si_nH_x$ clusters have also been examined by theoretical methods. Using the local density approximation, Hirao and Uda[51] found that the band gaps of hydrogenated silicon particles 7.3−15.5 Å in diameter ($Si_{10}H_{16}$−$Si_{123}H_{100}$) are 4.6−2.5 eV. According to these calculations, lattice distortions enhance the photoluminescence intensity for partially dehydrogenated clusters, while further dehydrogenation ultimately decreases the photoluminescence intensity. The results of these studies support the notion that the photoluminescence of porous silicon is due to $Si_nH_x$ particles. Similar studies by Onida and Andreoni[52] and by Rohlfing and Louie[56] have found similar evidence for the effects of structure on the optical properties of hydrogenated silicon clusters.

Despite these quite extensive experimental and theoretical studies, little is really known about the formation, structure, and stabilities of $Si_nH_x$ clusters. In this article, we describe studies of $Si_nH_x^+$, $n = 10-20$, clusters performed as a function of temperature. Our studies reveal information about the preferred [H]/[Si] ratios for these clusters, which is then used to infer information about their geometries. For $Si_nH_x^+$, $n = 10-20$ clusters, near stoichiometric compositions ($x \cong n$) are found to be prominent at intermediate temperatures. It is postulated that the stoichiometric clusters have Si−H units arranged in a cage-like geometries. Free energy calculations (using density functional theory) for a variety of $Si_nH_x$ compositions are found to be in qualitative agreement with the experimental results. For cluster cations with $n \geq 23$, $Si_nH_{(n-y)}^+$ ($y = 1-5$) clusters are found to be prominent at the higher temperatures. These hydrogen-depleted compositions may have Si−H cage geometries with one or more internal silicon atoms.

## Experimental Methods

Hydrogen-terminated silicon cluster cations are generated using a novel, laser photolysis source (Figure 1). The source is modular in design and consists of two sequential stainless steel regions connected by titanium tubes. The first block allows for the introduction of disilane ($Si_2H_6$) and subsequent photolysis by an excimer laser. A dilute mixture of disilane in helium (0.5% $Si_2H_6$/99.5% He, Voltaix, Inc.) is irradiated with the focused output of an excimer laser operating at 193 nm at 100 Hz. This results in the photolysis of the disilane and the initiation of $Si_nH_x$ cluster growth. Disilane has an absorption cross section between $4 \times 10^{-18}$ and $4 \times 10^{-19}$ cm$^2$ in the 190−200 nm wavelength region.[66] The growing $Si_nH_x$ clusters are then swept by a flowing He carrier gas (99.9999%) through a titanium connection tube into the second block, the annealing region, where the temperature can be varied between 300 and 1000 K.

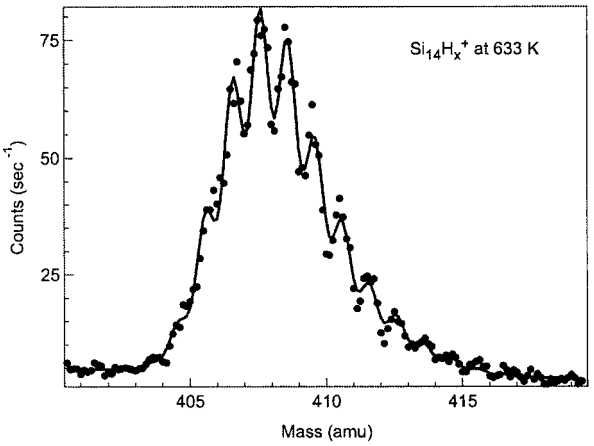


**Figure 2.** Mass spectrum recorded for $Si_{14}H_x^+$ at 633 K. The dots are the experimental data and the solid line is a least-squares fit using Gaussian functions.

The annealing region is heated by means of 2 mm diameter Thermocoax heating wire wrapped around the outside of the cylindrical annealing block. Approximately 400 W is required to obtain temperatures up to ∼1000 K. Helium buffer gas can be added to the annealing section to cause particle dilution and inhibit coalescence. In addition, small amounts of silicon tetrachloride, silicon tetrafluoride, or other halogen-containing gases can be introduced in this stage as etching reagents to assist in controlling nanocrystal formation.[67−71]

The cluster cations then enter a combined nozzle and ion optics assembly that allows for the formation and subsequent focusing of a cluster ion beam. No external ionization source is used, the cluster ions result from the photolysis laser. The cluster ions undergo a mild expansion through a conical nozzle into a low-vacuum chamber (base pressure $1 \times 10^{-8}$ Torr, operating pressure $4 \times 10^{-4}$ Torr) and are then focused into a low-energy ion beam. The cluster ion beam passes into a differentially pumped chamber and is then injected into a quadrupole mass spectrometer in a medium vacuum environment (base pressure $1 \times 10^{-8}$ Torr, operating pressure $6 \times 10^{-6}$ Torr). After mass analysis, the $Si_nH_x^+$ clusters are detected using dual microchannel plates.

## Results and Discussion

**$Si_nH_x^+$, $n = 10-20$.** Mass spectra were measured for $Si_nH_x^+$ ($n = 10-20$) clusters at temperatures of 301, 408, 633, 713, 787, 851, 898, and 943 K (all ±10 K). Figure 2 shows a mass spectrum recorded for $Si_{14}H_x^+$ at 633 K. Bare $Si_{14}^+$ would occur at $m/z \sim 393$ amu. In the spectrum there are peaks due to $Si_{14}H_x^+$ ($x = 11-24$). To obtain the hydrogen atom distribution, the measured mass spectra must be deconvoluted to remove the effects of the silicon isotope distribution ($^{28}$Si 92.23%, $^{29}$Si 4.67%, $^{30}$Si 3.10%). The solid line in Figure 2 is fit to the experimental data using Gaussian functions to represent the peaks. The intensity of each peak in the mass spectrum is given by the amount of $^{28}Si_{14}H_x$ present plus contributions from higher isotopes of clusters with fewer hydrogen atoms (for example: $^{29}Si^{28}Si_{13}H_{x-1}$, $^{30}Si^{28}Si_{13}H_{x-2}$, $^{29}Si_228Si_{12}H_{x-2}$, and so on). The hydrogen atom distribution is adjusted using a least-squares criterion to fit the measured mass spectrum. This procedure is repeated for each cluster ion, $Si_nH_x^+$ ($n = 10-20$) at each temperature.

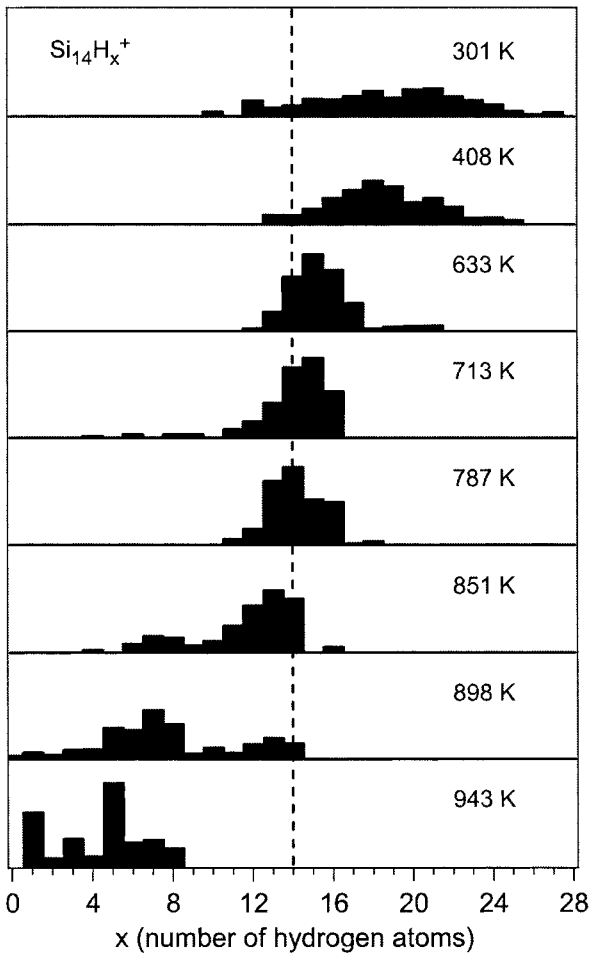


**Figure 3.** Hydrogen atom distribution obtained for $Si_{14}H_x^+$ as a function of annealing temperature.

For $n = 10-20$ the source produces hydrogen-rich cations ([H]/[Si] $\geq$ 1) at room temperature. Between ~408 and 633 K there is a transition to a near stoichiometric ([H]/[Si] $\cong$ 1) composition. The near stoichiometric composition persists between ~633 and 851 K. At temperatures above ~851 K, there is an abrupt transition to hydrogen-poor $Si_nH_x^+$ ions ([H]:[Si] < 1). The decrease in the hydrogen composition with increasing temperature can be viewed as the microscopic analogue of temperature-programmed desorption studies of hydrogen on bulk silicon surfaces. Figure 3 shows a plot of the hydrogen atom distributions obtained for $Si_{14}H_x^+$ as a function temperature. At low temperatures (301−408 K), there is a broad distribution of $x$ values. The cluster ions have a [H]/[Si] ratio between 1 and 2, which is lower than in the $Si_2H_6$ reagent ([H]/[Si] = 3) and other longer polysilane species ([H]/[Si] $\cong$ 2). However, there are enough hydrogen atoms to saturate all dangling bonds in a structure that has a bulklike silicon core. For example, for $Si_{14}$ an adamantane-like geometry with a second four atom cap at the bottom of the $Si_6$ chair is a plausible bulklike geometry. Termination of the surface dangling bonds for this geometry would lead to a $Si_{14}H_{20}$ composition. The broad distribution of $x$ values observed around room temperature, perhaps coincidentally, peaks around $x = 20$.

As the temperature is raised the hydrogen distribution narrows considerably and shifts to lower values. At 633−851 K the distribution is centered close to [H]/[Si] = 1 and has a width of only 3−4 hydrogens. The distribution changes only slightly over the 633−851 K temperature range. The shift to a [H]/[Si] of ~1 suggests that a structural transition has occurred. Similar average compositions were observed by Martin and Schaber for $Si_nH_x^+$ ($n \geq 11$) resulting from a discharge source.[4] As the temperature is raised the [H]/[Si] ratio continues to drop and ultimately approaches zero as only almost-bare $Si_n^+$ cluster ions remain. The results shown in Figure 3 for $Si_{14}H_x^+$ are representative of our results for all clusters with $n = 10-20$. In particular, the near stoichimetric composition exists at intermediate temperatures for all of these clusters.

The persistence of the near stoichiometric composition suggests that the $Si_nH_n$ composition is stable. The stability of this composition presumably has a structural origin. While it would be possible to construct a large variety of plausible geometries for a single value of n, the fact that the $Si_nH_n$ composition is favored for a broad range of $n$ severely limits the possible structures. Specifically, there must be a family of stable geometries with a common structural motif. The only geometries which seem to be compatible with the experimental observations are cage-like structures built from Si−H units arranged in four-, five-, and six-membered rings. These structures have nearly tetrahedral coordination at the $sp^3$ silicon atoms and can be viewed as the Si−H analogues of the carbon cage structures recently described by Jones.[72] A simple analysis of the thermochemistry of $Si_nH_x$ clusters suggests that $\Delta H$ for $H_2$ loss should increase significantly at the $x = n$ composition because at this point it is necessary to start making multiple Si−Si bonds, which is energetically unfavorable. This, and the stable cage-like structural motif, explains why the near stoichiometric composition is prevalent for clusters with $n = 10-20$.

To examine the relative stabilities of the stoichiometric cage geometries, density functional theory calculations were performed for a variety $Si_nH_x$ clusters with $n = 10$, 12, and 14. These calculations were performed using *Gaussian 94* (Revision D.4),[73] with the B3LYP (Becke three-parameter-Lee−Yang−Parr) functional and the 6-31+G(d,p) basis set. Recent investigations have shown that this hybrid B3LYP functional[74] reliably predicts the energetics of silicon hydride systems.[59,61] We have performed calculations on a number of plausible structures for hydrogen-rich, stoichiometric, and hydrogen-poor $Si_{14}H_x$ clusters, including (for comparison) the lowest-energy $Si_{14}$ structure recently reported.[75] The optimized geometries for $Si_{14}H_x$ are shown in Figure 4. These calculations were performed for neutral clusters while the experimental results were obtained for ions. However, recent computational studies for $n \leq 18$ show that the geometries of $Si_n^+$ cations generally resemble those of the corresponding neutrals (there are some small distortions and a minor reordering of the low energy geometries occurs for some cluster sizes).[76] Our preliminary calculations on $Si_{14}H_x^+$ ions suggest that the geometries of the $Si_nH_x$ clusters are also not strongly dependent on the charge state. Table 1 shows a comparison of the relative energies of the $Si_{14}H_x$ geometries shown in Figure 4. The energies of the different clusters were normalized using

$$E_{\text{norm}}(\text{Si}_n\text{H}_x) = E(\text{Si}_n\text{H}_x) + \left[\frac{x_{\max} - x}{2}\right]E(\text{H}_2)$$

where $E(Si_nH_x)$ and $E(H_2)$ are the calculated energies of the $Si_nH_x$ cluster and the $H_2$ molecule, respectively, and $x_{max}$ is the highest number of hydrogen atoms present for the $Si_nH_x$ cluster. The results in Table 1 show that the hydrogen-rich bulklike structures are more stable energetically than the stoichiometric and hydrogen-poor structures by 200−500 kJ $mol^{-1}$ and 1100−1200 kJ $mol^{-1}$, respectively. Similar results were found for the $Si_{10}H_x$ and $Si_{12}H_x$ clusters. The results of the calculations

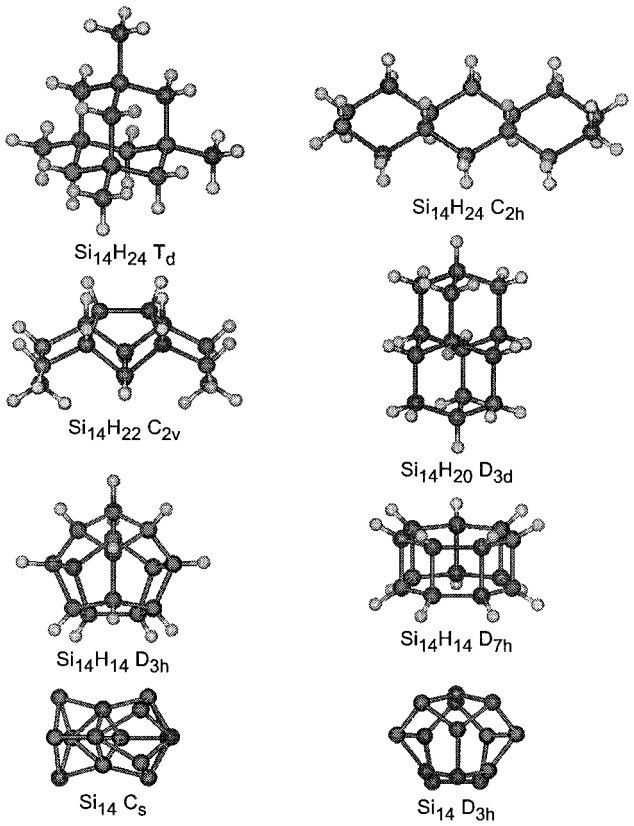


**Figure 4.** Local minima for neutral $Si_{14}H_x$ structures found using the B3LYP density functional formalism as implemented in *Gaussian 94* (Rev. D). The pruned 75 302 grid was used. Symmetry-constrained geometry optimizations were performed using the Berny algorithm with convergence criteria of 0.00045 and 0.00030 for the maximum component of the force and the root-mean-square for the forces, respectively. In each case, the final configuration was verified as a local minimum via a frequency calculation (there were no imaginary frequencies). The interconversion between isomers of similar energies was not investigated.

**TABLE 1: Relative Energies at 0 K for $Si_{14}H_x$ Clusters from DFT Calculations (see text for details)**

| cluster | relative energy, kJ/mol$^{-1}$ |
|---|---|
| $Si_{14}H_{24}$ $T_d$ | 0 |
| $Si_{14}H_{24}$ $C_{2h}$ | 22 |
| $Si_{14}H_{20}$ $D_{3d}$ | 35 |
| $Si_{14}H_{22}$ $C_{2v}$ | 51 |
| $Si_{14}H_{14}$ $D_{3h}$ | 235 |
| $Si_{14}H_{14}$ $D_{7h}$ | 486 |
| $Si_{14}$ $D_{3h}$ | 1178 |
| $Si_{14}$ $C_s$ | 1114 |

apparently do not provide an explanation for the transitions observed in the experiments.

The calculations described above fail to consider the effect of entropy. There is a substantial amount of translational entropy associated with the hydrogen molecules when they desorb from the $Si_nH_x$ clusters, and this makes a significant contribution to the free energies. Figure 5 shows relative Gibbs free energies (including translational, electronic, rotational, and vibrational contributions) for the six $Si_{14}H_x$ clusters shown in Figure 4 plotted against temperature. The free energies were calculated using an $H_2$ partial pressure of 0.1 Torr. This pressure was chosen to model the partial pressure of $H_2$ in the source which is not known exactly. The results shown in Figure 5 are not sensitive to the $H_2$ partial pressure. Near to room temperature the $Si_{14}H_{20}$ $D_{3d}$ bulklike fragment has the lowest free energy,

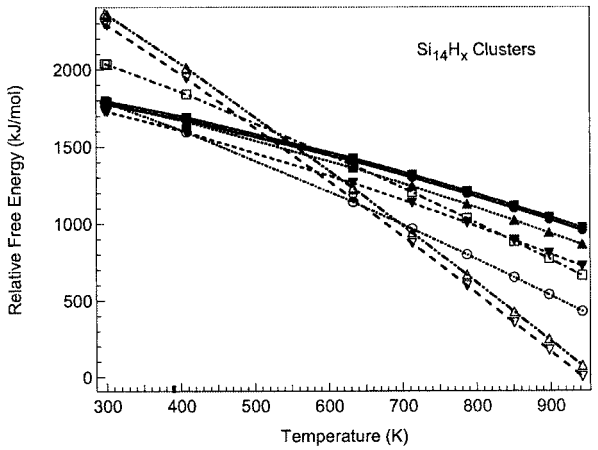


**Figure 5.** The normalized, relative Gibbs free energy versus temperature for $Si_{14}H_x$ clusters. Key: (●) $Si_{14}H_{24}$ $T_d$, (■) $Si_{14}H_{24}$ $C_{2h}$, (▲) $SiH_{22}$ $C_{2v}$, (▼) $Si_{14}H_{20}$ $D_{3d}$, (○) $Si_{14}H_{14}$ $D_{3h}$, (□) $Si_{14}H_{14}$ $D_{7h}$, (△) $Si_{14}$ $D_{3h}$, and (▽) $Si_{14}$ $C_s$.

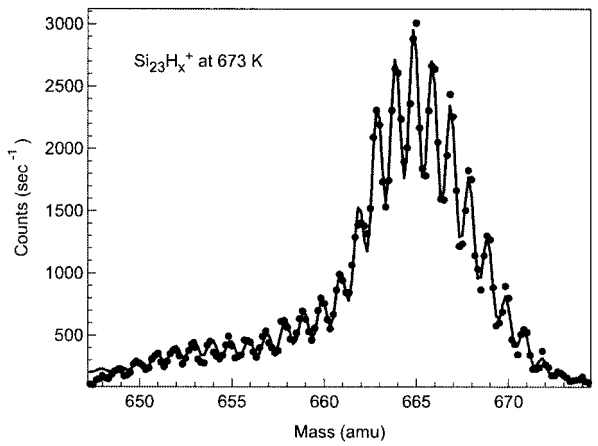


**Figure 6.** Mass spectrum recorded for $Si_{23}H_x^+$ at 673 K. The dots are the experimental data and the solid line is a least-squares fit using Gaussian functions.

though the other $Si_{14}H_x$ clusters with high [H]/[Si] ratios are close. However, for temperatures above approximately 410 K the $Si_{14}H_{14}$ $D_{3h}$ cage has the lowest free energy, and above around 650 K the bare $Si_{14}$ $C_s$ and $Si_{14}$ $D_{3h}$ clusters have the lowest free energies. The switch from hydrogen-rich clusters to stoichiometric to bare silicon clusters with increasing temperature is in qualitative agreement with the experiments. Similar behavior was found in the calculations for $Si_{10}H_x$ and $Si_{12}H_x$.

The inclusion of entropic factors results in qualitative agreement between the experimental observations and the thermochemical calculations. The entropic effects result primarily from the increase in the number of gaseous species that occurs as a result of dehydrogenation of the hydrogen-rich and stoichiometric clusters. At lower temperatures, the hydrogen-rich clusters are more stable energetically; conversely, at higher temperatures, entropy becomes more important and the formation of hydrogen poor $Si_nH_x$ and/or bare $Si_n$ clusters is favored. A similar observation has been reported in recent thermochemical studies of silicon hydride cluster formation during the thermal decomposition of silane.[45]

**$Si_nH_x^+$, $n = 20-30$.** Mass spectra were measured for $Si_nH_x^+$ ($n = 20-30$) clusters at temperatures of 303, 373, 473, 573, 673, 773, and 873 K (all ±5 K). Figure 6 shows a mass spectrum recorded for $Si_{23}H_x^+$ at a temperature of 673 K. Bare $Si_{23}^+$ would occur at $m/z \sim 646$ amu. In the spectrum there are peaks

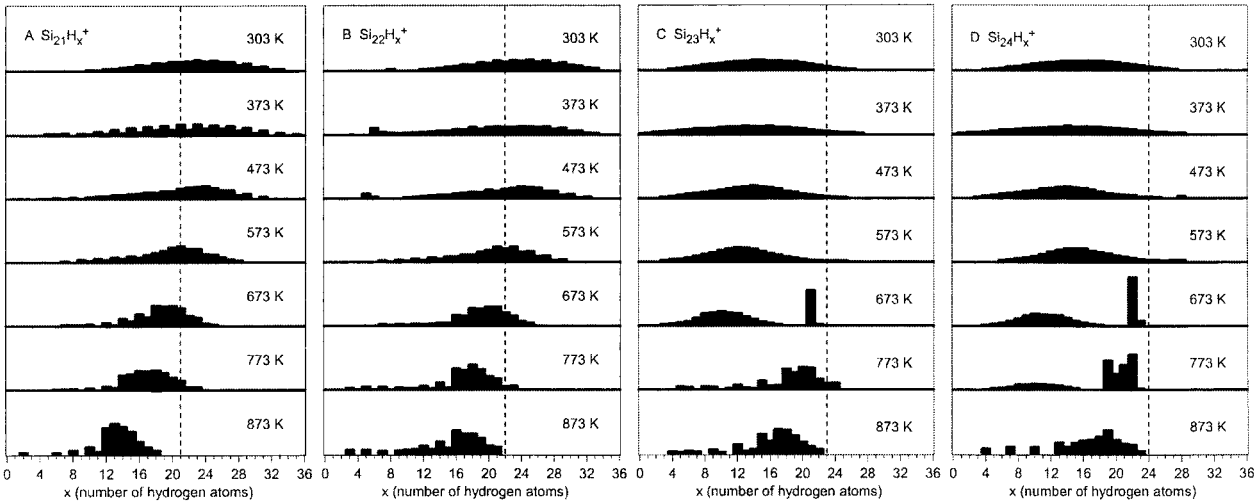


**Figure 7.** Hydrogen atom distribution obtained $Si_{21}H_x^+$ (A), $Si_{22}H_x^+$ (B), $Si_{23}H_x^+$ (C), and $Si_{24}H_x^+$ (D) as a function of annealing temperature.

due to $Si_{23}H_x^+$ ($x = 4-30$). As described above, the measured mass spectra must be deconvoluted to remove the effects of the silicon isotope distribution in order to obtain the hydrogen atom distribution. The solid line in Figure 6 is the fit to the experimental data using the approach described above for the smaller clusters.

Figure 7 shows plots of the hydrogen atom distributions obtained for $Si_{21}H_x^+$ (A), $Si_{22}H_x^+$ (B), $Si_{23}H_x^+$ (C), and $Si_{24}H_x^+$ (D) as a function temperature. Hydrogen-rich cations ([H]/[Si] $\geq$ 1) are produced at room temperature for $Si_nH_x^+$ clusters with $n = 20-22$. At low temperatures (303−473 K), there is a broad distribution of $x$ values. Between ∼473 and 573 K, the maximum in the hydrogen atom distribution becomes centered near a stoichiometric ([H]/[Si] $\cong$ 1) composition. The near stoichiometric composition persists between ∼573 and 773 K. At temperatures above ∼773 K, there is a transition to hydrogen-poor $Si_nH_x^+$ ions ([H]:[Si] < 1). As the temperature is raised the [H]/[Si] ratio continues to decrease. These results are in qualitative agreement with those described above for $Si_nH_x^+$ with $n = 10-20$.

An abrupt transition occurs for $Si_nH_x^+$ clusters with $n = 23$, and for clusters with $n = 23-30$ the source primarily produces hydrogen-poor cations ([H]/[Si] $\leq$ 1) at room temperature. At low temperatures (303−473 K), there is a broad distribution of $x$ values. Between ∼573 and 673 K, the hydrogen atom distribution becomes bimodal. One peak corresponds to a range of hydrogen-poor $Si_nH_x^+$ ions ([H]/[Si] < 1), and the other peak is centered around a $Si_nH_{(n-2)}^+$ composition. These distributions persist between ∼673 and 773 K. At temperatures above ∼773 K, the two distributions coalesce and a transition to primarily hydrogen poor $Si_nH_x^+$ ions ([H]/[Si] < 1) occurs. As the temperature is raised the [H]/[Si] ratio continues to decrease. The behavior of clusters with $n \geq 23$ is thus quite different from that for $Si_nH_x^+$ with $n = 10-22$.

A series of experiments were performed to examine the effects of the disilane concentration on the composition of the clusters. Figure 8 shows a mass spectrum recorded for $Si_{23}H_x^+$ at a temperature of 673 K with an elevated disilane concentration (the flow of the dilute mixture of disilane in helium was increased to equal that of the helium carrier gas). The mass spectrum was fit using the procedure described above. Note the decrease in hydrogen-poor $Si_nH_x^+$ cation clusters in comparison with the mass spectrum shown in Figure 6. Figure 9 shows plots of the hydrogen atom distributions obtained for $Si_{23}H_x^+$ (A) and $Si_{24}H_x^+$ (B) as a function of temperature. Unlike the results

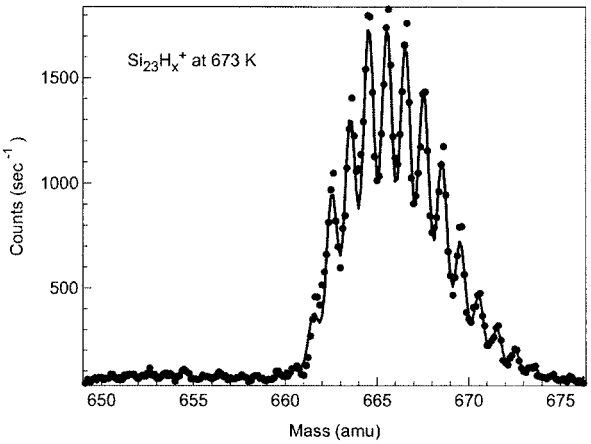


**Figure 8.** Mass spectrum recorded for $Si_{23}H_x^+$ at 673 K. The dots are the experimental data and the solid line is a least-squares fit using Gaussian functions. Note the decrease in hydrogen-poor $Si_nH_x^+$ cation clusters below ∼660 amu with respect to mass spectrum shown in Figure 6.

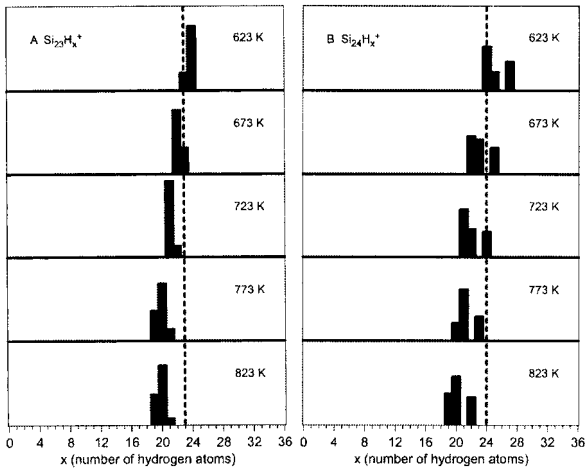


**Figure 9.** Hydrogen atom distribution obtained $Si_{23}H_x^+$ (A) and $Si_{24}H_x^+$ (B) as a function of annealing temperature (with an elevated disilane concentration).

presented in Figure 7, these clusters ions have a narrow distribution of $x$ values, in some cases only one or two hydrogens wide. At 623 K, the cluster cations have a [H]/[Si] ratio slightly greater than 1, and at 673 K the hydrogen atom distribution becomes centered near the stoichiometric ([H]/[Si]

$\cong$ 1) composition. At temperatures greater than 673 K, the distribution shifts to become slightly hydrogen poor ([H]/[Si] $\leq$ 1). At 723 K, the hydrogen atom distribution correspond to the formula $Si_nH_{(x-2)}^+$. A similar composition occurs in Figure 7 at $T = 673$ K. At temperatures between 723 and 823 K, the hydrogen atom distributions in Figure 9 are centered around $x$ values corresponding to ions with formulas between $Si_nH_{(n-1)}^+$ and $Si_nH_{(n-5)}^+$. These studies show that the width and the position of the hydrogen atom distribution can be shifted by adjusting the flow of $Si_2H_6$ as well as by changing the temperature of the cluster source.

The results presented in Figures 3 and 7 show that a shift in the hydrogen atom distribution occurs for $Si_nH_x^+$ ions at intermediate temperatures. For the smaller clusters the near stoichiometric compositions ($x \cong n$) persists throughout the intermediate temperature range. As discussed above, these stoichiometric clusters presumably have Si−H units arranged in cage-like geometries. For the larger clusters the stoichiometric composition persists over a narrower temperature range, and hydrogen-depleted compositions appear to be favored. It is possible that these clusters consist of a cage made of Si−H units with one or more internal silicon atoms. These structures can be viewed as hydrogenated analogues of the types of structures proposed by Rothlisberger, Andreoni, and Parrinello for bare silicon clusters.[77] The stabilities of bare and hydrogenated silicon cages containing internal silicon have been investigated using a variety of theoretical methods.[58,78,79]

It is interesting to note that previous research on bare silicon clusters cations has shown that a structural transition occurs for clusters cations containing between 23 and 27 silicon atoms.[80,81] However, it seems unlikely that the transition observed with the hydrogenated silicon clusters at $n = 23$ is related to the structural rearrangements observed with bare silicon clusters for $n = 23-27$.

## Conclusions

The synthesis of $Si_nH_x^+$ ($n = 10-30$) clusters has been studied as a function of temperature using mass spectrometry. For $Si_nH_x^+$ clusters with $n = 10-22$, near stoichiometric compositions ($x \cong n$) are prominent at intermediate temperatures. The stoichiometric clusters probably have Si−H units arranged in a cage-like geometry. Free energy calculations using DFT normalized energies for a variety of $Si_nH_x$ compositions are in qualitative agreement with the experimental results. Comparisons between experiment and theory requires consideration of free energies of the $Si_nH_x$ species, not simply the calculation of the electronic energies at 0 K. At $n = 23$ an abrupt transition occurs, and hydrogen-rich clusters are not observed at low temperatures. For clusters with $n \geq 23$, hydrogen-depleted structures with formulas between $Si_nH_{(n-1)}^+$ and $Si_nH_{(n-5)}^+$ are found at the higher temperatures. These clusters may have structures consisting of hydrogen-depleted Si−H cages with one or more internal silicon atoms. Under some source conditions the distribution of hydrogen atoms on the larger cluster can be as small as one or two hydrogens.

**Acknowledgment.** This work was funded by the National Science Foundation and by a multidisciplinary university research initiative (MURI) grant (DAAG-55-97-0133) from the Army Research Office. In addition, the authors thank G. C. Schatz for many helpful discussions, and R. O. Jones and K. M. Ho for supplying coordinates for a variety of structures.

## References and Notes

(1) Canham, L. T. *Appl. Phys. Lett.* **1990**, *57*, 1046−1048.
(2) Cullis, A. G.; Canham, L. T.; Calcott, P. D. J. *J. Appl. Phys.* **1997**, *82*, 909−965.
(3) Haller, I. *Appl. Phys. Lett.* **1980**, *37*, 282−284.
(4) Martin, T. P.; Schaber, H. *J. Chem. Phys.* **1985**, *83*, 855−858.
(5) Lowndes, D. H.; Geohegan, D. B.; Eres, D.; Pennycook, S. J.; Mashburn, D. N.; Jellison, G. E., Jr. *Appl. Phys. Lett.* **1988**, *52*, 1868−1870.
(6) Mandich, M. L.; Reents, W. D., Jr.; Kolenbrander, K. D. *J. Vac. Sci. Technol. B* **1989**, *7*, 1295−1302.
(7) Eres, D.; Geohegan, D. B.; Lowndes, D. H.; Mashburn, D. N. *Appl. Surf. Sci.* **1989**, *36*, 70−80.
(8) Gates, S. M.; Greenlief, C. M.; Beach, D. B. *J. Chem. Phys.* **1990**, *93*, 7493−7503.
(9) Giunta, C. J.; McCurdy, R. J.; Chapple-Sokol, J. D.; Gordon, R. G. *J. Appl. Phys.* **1990**, *67*, 1062−1075.
(10) Simon, J.; Feurer, R.; Reynes, A.; Morancho, R. *J. Anal. Appl. Pyrolysis* **1992**, *24*, 51−59.
(11) Fowler, B.; Lian, S.; Krishnan, S.; Jung, L.; Li, C.; Banerjee, S. *J. Electrochem. Soc.* **1992**, *139*, 2314−2318.
(12) Okada, T.; Nishimi, A.; Shibamura, N.; Maeda, M. *Jpn. J. Appl. Phys.* **1992**, *31*, 3707−3711.
(13) Jasinski, J. M.; Becerra, R.; Walsh, R. *Chem. Rev.* **1995**, *95*, 1203−1228.
(14) Hollenstein, C.; Schwarzenbach, W.; Howling, A. A.; Courteille, C.; Dorier, J.-L.; Sansonnens, L. *J. Vac. Sci. Technol. A* **1996**, *14*, 535−539.
(15) Kessels, W. M. M.; van de Sanden, M. C. M.; Schram, D. C. *Appl. Phys. Lett.* **1998**, *72*, 2397−2399.
(16) Marra, D. C.; Edelberg, E. A.; Naone, R. L.; Aydil, E. S. *J. Vac. Sci. Technol. A* **1998**, *16*, 3199−3210.
(17) Satake, K.; Inoue, Y.; Ukai, O.; Takeuchi, Y. *Appl. Phys. Lett.* **1998**, *73*, 1799−1801.
(18) Hasegawa, S.; Sakata, M.; Inokuma, T.; Kurata, Y. *J. Appl. Phys.* **1998**, *84*, 584−588.
(19) Tada, N.; Tonokura, K.; Matsumoto, K.; Koshi, M.; Miyoshi, A.; Matsui, H. *J. Phys. Chem. A* **1999**, *103*, 322−329.
(20) Jasinski, J. M.; LeGoues, F. K. *Chem. Mater.* **1991**, *3*, 989−992.
(21) Heath, J. R.; Jasinski, J. M. *Mater. Res. Soc. Symp. Proc.* **1992**, *256*, 117−122.
(22) Littau, K. A.; Szajowski, P. J.; Muller, A. J.; Kortan, A. R.; Brus, L. E. *J. Phys. Chem.* **1993**, *97*, 1224−1230.
(23) Brus, L. *J. Phys. Chem.* **1994**, *98*, 3575−3581.
(24) Murakami, H.; Kanayama, T. *Appl. Phys. Lett.* **1995**, *67*, 2341−2343.
(25) Guyot, Y.; Champagnon, B.; Boudeulle, M.; Melinon, P.; Prevel, B.; Bupuis, V.; Perez, A. *Thin Solid Films* **1997**, *297*, 188−191.
(26) Xu, C.; Taylor, T. R.; Burton, G. R.; Neumark, D. N. *J. Chem. Phys.* **1998**, *108*, 7645−7652.
(27) Schulze, G.; Henzler, M. *Surf. Sci.* **1983**, *124*, 336−350.
(28) Abrefah, J.; Olander, D. R. *Surf. Sci.* **1989**, *209*, 291−313.
(29) Wolff, S. H.; Wagner, S.; Bean, J. C.; Hull, R.; Gibson, J. M. *Appl. Phys. Lett.* **1989**, *55*, 2017−2019.
(30) Wu, B. R.; Cheng, C. *J. Phys.: Condens. Matter* **1994**, *6*, 1113−1124.
(31) Watanabe, M. O.; Murakami, H.; Miyazaki, T.; Kanayama, T. *Appl. Phys. Lett.* **1997**, *71*, 1207−1209.
(32) Agrawal, P. M.; Thompson, D. L.; Raff, L. M. *J. Chem. Phys.* **1990**, *92*, 1069−1082.
(33) Raghavachari, K. *J. Chem. Phys.* **1990**, *92*, 452−465.
(34) Raghavachari, K. *J. Chem. Phys.* **1991**, *95*, 7373−7388.
(35) Curtis, L. A.; Raghavachari, K.; Deutsch, P. W.; Pople, J. A. *J. Chem. Phys.* **1991**, *95*, 2433−2444.
(36) Raghavachari, K. *J. Chem. Phys.* **1992**, *96*, 4440−4448.
(37) Marshall, P. *J. Mol. Struct.* **1994**, *313*, 19−25.
(38) Michels, H. H.; Hobbs, R. H. *Chem. Phys. Lett.* **1993**, *207*, 389−396.
(39) Zachariah, M. R.; Carrier, M. J.; Blaisten-Barojas, E. *J. Phys. Chem.* **1996**, *100*, 14856−14864.
(40) Greeff, C. W.; Lester, W. A. J. *J. Chem. Phys.* **1997**, *106*, 6412−6417.
(41) Katzer, G.; Ernst, M. C.; Sax, A. F.; Kalcher, J. *J. Phys. Chem. A* **1997**, *101*, 3942−3958.
(42) Hong, S.; Chou, M. Y. *Phys. Rev. B* **1998**, *58*, R13363−R13366.
(43) Ramalingam, S.; Maroudas, D.; Aydil, E. S. *Appl. Phys. Lett.* **1998**, *72*, 578−580.
(44) Ramalingam, S.; Maroudas, D.; Aydil, E. S. *J. Appl. Phys.* **1998**, *84*, 3895−3911.
(45) Swihart, M. T.; Girshick, S. L. *J. Phys. Chem. B* **1999**, *103*, 64−76.
(46) Brown, A. R.; Doren, D. J. *J. Chem. Phys.* **1999**, *110*, 2643−2651.
(47) Ramalingam, S.; Mahalingam, P.; Aydil, E. S.; Maroudas, D. *J. Appl. Phys.* **1999**, *86*, 5497−5508.

(48) Ramalingam, S.; Maroudas, D.; Aydil, E. S. *J. Appl. Phys.* **1999**, *86*, 2872−2888.
(49) Ramalingam, S.; Maroudas, D.; Aydil, E. S. *IEEE Trans. Plasma Sci.* **1999**, *27*, 104−105.
(50) Swihart, M. T. *J. Phys. Chem. A* **2000**, *104*, 6083−6087.
(51) Hirao, M.; Uda, T. *Surf. Sci.* **1994**, *306*, 87−92.
(52) Onida, G.; Andreoni, W. *Chem. Phys. Lett.* **1995**, 243.
(53) Miyazaki, T.; Uda, T.; Stich, I.; Terakura, K. *Chem. Phys. Lett.* **1996**, *261*, 346−352.
(54) Miyazaki, T.; Uda, T.; Stich, I.; Terakura, K. *Chem. Phys. Lett.* **1998**, *284*, 12−18.
(55) Sun, Q.; Yu, J. Z.; Zhou, L.; Li, Z. Q.; Tang, Z.; Ohno, K.; Kawazoe, Y. *Europhys. Lett.* **1998**, *43*, 47−52.
(56) Rohlfing, M.; Louie, S. G. *Phys. Rev. Lett.* **1998**, *80*, 3320−3323.
(57) Meleshko, V.; Morokov, Y.; Schweigert, V. *Chem. Phys. Lett.* **1999**, *300*, 118−124.
(58) Martonak, R.; Molteni, C.; Parrinello, M. *Phys. Rev. Lett.* **2000**, *84*, 682−685.
(59) Nachtigall, P.; Jordan, K. D.; Sosa, C. *J. Phys. Chem.* **1993**, *97*, 11666−11672.
(60) Radeke, M. R.; Carter, E. A. *Phys. Rev. B* **1996**, *54*, 11803−11817.
(61) Nachtigall, P.; Jordan, K. D.; Smith, A.; Jonsson, H. *J. Chem. Phys.* **1996**, *104*, 148−158.
(62) Kohen, D.; Tully, J. C.; Stillinger, F. H. *Surf. Sci.* **1998**, *397*, 225−236.
(63) Nakajima, K.; Miyazaki, K.; Koinuma, H.; Sato, K. *J. Appl. Phys.* **1998**, *84*, 606−610.
(64) Hansen, U.; Vogl, P. *Phys. Rev. B* **1998**, *57*, 13295−13304.
(65) Earley, C. W. *J. Phys. Chem. A* **2000**, *104*, 6622−6627.
(66) Itoh, U.; Toyoshima, Y.; Onuki, H.; Washida, N.; Ibuki, T. *J. Chem. Phys.* **1986**, *85*, 4867−4872.
(67) Janai, M.; Aftergood, S.; Weil, R. B.; Pratt, B. *J. Electrochem. Soc.* **1981**, *128*, 2660−2665.
(68) Bloem, J.; Oei, Y. S.; Moor, H. H. C. d.; Hanssen, J. H. L.; Giling, L. J. *J. Electrochem. Soc.* **1985**, *132*, 1973−1980.
(69) Flamm, D. L. *Pure Appl. Chem* **1990**, *62*, 1709−1720.
(70) Hiroi, M.; Tatsumi, T. *Jpn. J. Appl. Phys.* **1994**, *33*, 2244−2247.
(71) Karahashi, K.; Matsuo, J.; Horiuchi, K. *Jpn. J. Appl. Phys.* **1994**, *33*, 2252−2254.
(72) Jones, R. O. *J. Chem. Phys.* **1999**, *110*, 5189−5200.
(73) Frisch, M. J.; Trucks, G. W.; Schlegel, H. B.; Gill, P. M. W.; Johnson, B. G.; Robb, M. A.; Cheeseman, J. R.; Keith, T.; Petersson, G. A.; Montgomery, J. A.; Raghavachari, K.; Al-Laham, M. A.; Zakrzewski, V. G.; Ortiz, J. V.; Forseman, J. B.; Cioslowski, J.; Stefanov, B. B.; Nanayakkara, A.; Challacombe, M.; Peng, C. Y.; Ayala, P. Y.; Chen, W.; Wong, M. W.; Andres, J. L.; Replogle, E. S.; Gomperts, R.; Martin, R. L.; Fox, D. J.; Binkley, J. S.; Defrees, D. J.; Baker, J.; Stewart, J. P.; Head-Gordon, M.; Gonzalez, C.; Pople, J. A. *Gaussian 94*, Revision D.4 ed.; Gaussian, Inc.: Pittsburgh, PA, 1995.
(74) Becke, A. D. *J. Chem. Phys.* **1993**, *98*, 5648−5652.
(75) Ho, K. M.; Shvartsburg, A. A.; Pan, B.; Li, Z. Y.; Wang, C. Z.; Wacker, J. G.; Fye, J. L.; Jarrold, M. F. *Nature* **1998**, *392*, 582−585.
(76) Liu, B.; Lu, Z.-Y.; Pan, B.; Wang, C.-Z.; Ho, K.-M.; Shvartsburg, A. A.; Jarrold, M. F. *J. Chem. Phys.* **1998**, *109*, 9401−9409.
(77) Rothlisberger, U.; Andreoni, W.; Parrinello, M. *Phys. Rev. Lett.* **1994**, *72*, 665−668.
(78) Menon, M.; Subbaswamy, K. R. *Phys. Rev. B* **1995**, *51*, 17952−17956.
(79) Gong, X. G. *Phys. Rev. B* **1995**, *52*, 14677−14681.
(80) Jarrold, M. F.; Constant, V. A. *Phys. Rev. Lett.* **1991**, *67*, 2994−2997.
(81) Hudgins, R. R.; Imai, M.; Jarrold, M. F.; Dugourd, P. *J. Chem. Phys.* **1999**, *111*, 7865−7870.